Journal of Robotics and Control (JRC)
Volume 5, Issue 5, 2024
ISSN: 2715-5072, DOI: 10.18196/jrc.v5i5.22985

Dynamic Motion Control of Two-Link Robots with Adaptive Synergetic Algorithms

Aya Khudhair Abbas [1*], Saleem Khalefa Kadhim [2]
[1, 2] Department of Control and System Engineering, University of Technology-Iraq, Baghdad 10066, Iraq
Email: [1] cse.22.07@grad.uotechnology.edu.iq
*Corresponding Author

***Abstract*—Robotics is advancing to assist with daily tasks by developing human-like robotic limbs, which involves challenges in integrating software, control systems, electronics, and mechanical designs. To address these challenges, Classic Synergetic Controller (CSC) and Adaptive Synergetic Controller (ASC) algorithms were created using mathematical equations to regulate the robot arm's joint angle position and achieve precise tracking. A comparison with Adaptive Sliding Mode Control (ASMC) and Classical Sliding Mode Control (CSMC) demonstrated that CSC and ASC outperform in efficiency and robustness. ASC improved by 63%, providing smoother angular position tracking and faster response times. CSC reached the desired position angle in 1.5 seconds with oscillations, while ASC achieved it in 2.4 seconds without oscillations and eliminated chattering. CSC's Root Mean Square (RMS) was 1.57 rad, whereas ASC had no RMS value. The improvement rate of ASC over CSC was 100%, ensuring seamless motion, better rise time, and eliminating oscillations, thus providing robust control against disturbances and parameter variations.**

Keywords—Synergetic Controller; Adaptive Synergistic Controller; Robotic Manipulators; Two Degrees of Freedom; Chattering.

I. INTRODUCTION

Robotic manipulators are crucial in manufacturing due to their speed and precision and are increasingly used in daily life, impacting the production of nearly all products. Rapid, accurate movements of robotic arms pose a significant challenge in robotics. The complex dynamics of robot arms make them ideal for studying nonlinear programming. Two-link manipulators, resembling human limbs with Two Degrees of Freedom (2-DoF), help understand the complexities of human manipulation capabilities [1]. Therefore, controlling robot manipulators is challenging due to their complex dynamics, which involve nonlinear interactions between joint torques and arm positions. The presence of these nonlinear dynamics and coupling relationships makes precise and robust control difficult, making the development of effective controllers using standard methods a demanding task [2].

Within the Lagrangian framework, the energies influential and the innate duality of kinetic perfection are clarified. The torque applied in each cycle is calculated by using the Euler-Lagrange equation. [3]. The system's actions and functions are simulated using the CSC and ASC.

Synergetic control is A technique intended for nonlinear systems and offers a means of creating a stable control system that can manage nonlinearities and uncertainties. Control in nonlinear systems is challenging because of uncertainties and disturbances because there is a lack of proportionality between input and output variables. CSC successfully handles these difficulties [4]. The theoretical foundation of the CSC method is the study of complex systems with emergent properties. Furthermore, it illustrates how to work the system to obtain the desired angles.

Furthermore, controlling and resolving uncertainties that develop in the Robot system's parameters is the main goal of the ASC design. The adaptive control algorithm is intended to lessen the detrimental effects of disruptions, which may impair tracking efficiency. Therefore, in this work introduces an adaptive scheme grounded in the synergetic control notion to develop adaptive algorithms that are capable of predicting and reducing the impact of uncertainties in parameters. Additionally, this methodology is designed to ensure the stability of the system under control.

Several researchers have investigated the 2-DoF robot movement using different control methods. Therefore, the construction of an advanced CSC and ASC for evaluating the 2-DoF robot performance.

The literature on robotic control systems highlights various approaches to address these challenges. While Popov [5] explores synergetic control and its applications, and there are extensive studies on Sliding Mode Control (SMC) and its variations, there seems to be a lack of research on combining these two approaches to leverage the benefits of both in robotic control systems. Also, most studies, such as those by Baccouch and Dodds [6], and Jalani et al. [7], focus on simulations to verify theoretical findings. There is a need for more empirical research and real-world testing to validate these control strategies under practical conditions. In addition, Lochan and Roy [8] discuss the significance and drawbacks of different control techniques. However, there is limited comparative analysis in real-world scenarios to determine the most effective control strategy for specific applications, such as industrial robotics, medical devices, and Unmanned Aerial Vehicles (UAVs). However, Herrmann et al. [9] and Jalani et al. [7] touch on compliance control for grasping tasks. However, there is limited research on advanced human-robot interaction techniques, especially in collaborative environments where robots work alongside humans. Also, the existing studies mainly focus on control accuracy and robustness. There is a gap in exploring energy efficiency and optimization of control algorithms to enhance the longevity and operational cost-effectiveness of robotic

systems. Although, the review does not address the challenges and strategies for coordinating multiple robots working together on complex tasks, which is a growing area of interest in robotics. While adaptive control schemes are mentioned, there is a gap in exploring long-term adaptability and learning in control systems. This includes how robots can continually learn and adapt to new tasks and environments over time without human intervention. Identifying and addressing these gaps could lead to significant advancements in the field of robotic control systems, enhancing their efficiency, robustness, and applicability in various real-world scenarios.

SMC is a highly effective robust nonlinear controller known for its insensitivity to parameter uncertainty and external disruptions. It gained significant attention in the late 1970s for its systematic design process, which involves selecting a stable sliding surface and establishing a discontinuous control rule to guide the system's state to and maintain it on the sliding surface [10][11]. To address the chattering phenomenon and fine-tune controller gains, several technical approaches have been introduced, including the Integral Sliding Mode controller and Sliding Mode Fuzzy controller (FL), which aim for asymptotic stability. The ASMC has been proposed to enhance robustness and effectively reduce chattering, minimizing control effort without requiring prior knowledge of the system's upper bound [12][13].

Numerous literature uses different sliding mode control systems approaches, such Labbadi and Cherkaoui [14] they combines SMC methods with the Adaptive Backstepping approach, through examined a robust, adaptive controller for tracking and stabilizing the flight path of quadrotor UAVs. They used the Newton-Euler method to determine the dynamics of the quadrotor and created two sturdy controllers to control parametric uncertainties. Also, Zaihidee et al. [15] investigated cutting-edge SMC applications for Permanent Magnet Synchronous Motor (PMSM) speed control and Jung et al. [16] was tested A neuro-sliding mode control approach using a reference compensation technique in a non-model-based control framework and a stability analysis of the neuro-sliding mode control scheme was carried out, and simulation results showed that it outperformed traditional sliding mode control in tracking performance.

Fan et al. [17] suggested an adaptive grasp technique that uses error estimation compensation and collaboration control to mitigate object pose uncertainty. The outcomes demonstrate that this adaptive grasp strategy greatly raises the success rate of grasping objects in uncertain poses. Proposed a new object-level impedance control framework aimed at improving grasp force and quality by Li et al. [18], By dynamically sliding from the initial to the final grasp configuration, optimal grasp quality is achieved. The proposed controller allows the object to be maneuvered in hand while responding to external forces. Also Shahriari et al. [19] developed a single-arm control policy that applies to all robots in a multi-manual system, including an adaptive force-impedance controller based on a modeled control objective. In addition, Zhang et al. [20] proposed adaptive sliding mode friction indemnification adaptive impedance controllers for a stereophonic artificial hand. According to experimental results, in uncertain environments with unknown stiffness and position, the adaptive controller with friction indemnification was able to achieve accurate force-tracking and stable torque/force response. Also, Mahdi et al. [21] created an adaptive control architecture for path tracking based on synergy Control of joint position in a knee rehabilitation program. They created control laws and an adaptive SC and Adaptive SC scheme to guarantee the stabilization of the knee exoskeleton system when confronted with an input uncertainty. The Shadow Robot Company [22] created the Shadow Dexterous Hand, a humanoid robotic hand system with 24 movements that closely resembles the dexterity and kinematics of a human hand. PID controllers are configured during setup, and control strategies are implemented via EtherCAT.

While significant advancements have been made in control strategies for robotic manipulators, there remains a challenge in effectively controlling underactuated manipulators, especially in terms of mitigating the chattering effect inherent in robust control methods like SMC and ASMC. Existing approaches, including Proportional – Integral – Derivative (PID), FLC, and computed torque control, have their own benefits and limitations but do not fully address the chattering issue or the complexities associated with nonlinear systems and input uncertainties. Further research is needed to develop robust control strategies that can handle these challenges, ensuring stability and precision in underactuated manipulator systems.

Previous studies have not explored the application of CSC and ASC in manipulator robot motion, potentially offering improved stability and minimizing chattering. Excessive chattering could lead to damage to the manipulator of the robot. There is currently a lack of research examining the effectiveness of CSC, and ASC algorithms specifically for manipulators of robot control.

Therefore, this work presents a CSC to control the variables of a constrained underactuated robotic manipulator, aiming to maintain system robustness amid parameter variations and disturbances. Also, it involves analyzing the dynamic model and state space representation of the robotic manipulator, developing CSC algorithms, and conducting stability analysis based on the control law to ensure consistent and stable motion of the manipulator

The major advantages of the suggestion of CSC are:

- CSC provides robust control against disturbances and parameter variations, ensuring stable performance in dynamic and uncertain environments [4].
- CSC algorithms enable precise regulation of system states, which is crucial for controlling complex and underactuated robotic systems [5].
- CSC effectively manages nonlinear dynamics, making it suitable for systems with complex interactions and constraints [6].
- By analyzing the dynamic model and state-space representation, CSC helps maintain system stability even in the presence of disturbances [7].

- CSC can be tailored to various system configurations and requirements, enhancing its applicability across different robotic systems and manipulations.

As mentioned above we could include scalability to more complex robotic systems, real-world implementation challenges such as prosthetic fingers, and prosthetic hand, or enhancements in control algorithms.

This paper will include the following sections in a sequential order:

- The dynamics and control model outlines the mathematical model of a 2-DoF robot actuated by CSC and ASC.
- Results and discussion display simulation results and a discussion of the control system and model response.
- Finally, the paper is concluded with a section titled Conclusion. The methodology of this paper is described in the block diagram shown in Fig. 1, which depicts the sequence of presenting the contents of this research.

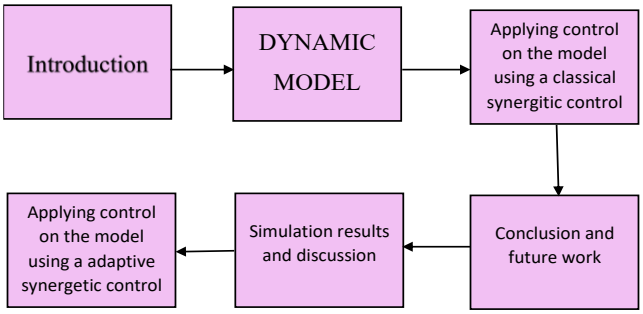

Fig. 1. Block diagram of the methodology

II. DYNAMICS MODEL

Advancements in robotics have greatly enhanced productivity and efficiency in the automation industry, where robots perform a range of tasks including cutting, welding, assembling, and picking and placing [23]. Fig. 2 shows the free body diagram to the robotic arm on which the control methods are applied. A two-dimensional (2-D) 2-DOF robot was viewed as a movable belt made up of two cylindrical links.

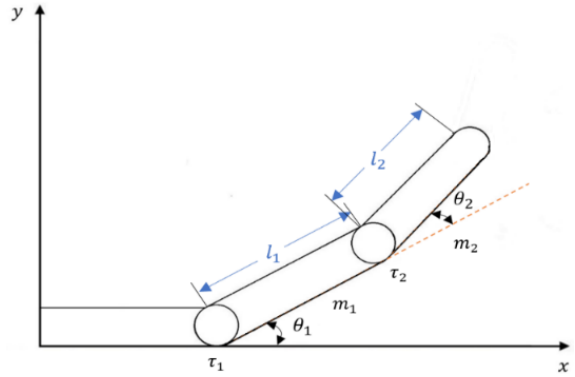

Fig. 2. Schematic diagram for the two-link robot manipulator

The 2-DOF robot displacement is represented by X and Y in cartesian coordinates, whereas the angular displacement of the 2-DOF robot links is denoted by θ. The displacement equations for first link are as follows,

$$\left.\begin{aligned} x_1 &= l_1 \cos\theta_1 \\ y_1 &= l_1 \sin\theta_1 \end{aligned}\right\} \quad (1)$$

Where θ_1 is the first link angular displacement, and l_1 represents the length of the first link. Also, the displacement for the second link as:

$$\left.\begin{aligned} x_2 &= l_1 \cos\theta_1 + l_2 \cos(\theta_1 + \theta_2) \\ y_2 &= l_1 \sin\theta_1 \ + l_2 \sin(\theta_1 + \theta_2) \end{aligned}\right\} \quad (2)$$

By deriving Equations (1) and (2) concerning time, which allows the linear velocities at each link to be obtained as follows:

$$\left.\begin{aligned} \dot{x_1} &= -l_1\dot{\theta}_1 \sin\theta_1 \\ \dot{y_1} &= \ l_1\dot{\theta}_1 \cos\theta_1 \end{aligned}\right\} \quad (3)$$

$$\left.\begin{aligned} \dot{x_2} &= -l_1\dot{\theta}_1 \sin\theta_1 - l_2(\dot{\theta}_1 + \dot{\theta}_2)\sin(\theta_1 + \theta_2) \\ \dot{y_2} &= \ l_1\dot{\theta}_1 \cos\theta_1 + l_2(\dot{\theta}_1 + \dot{\theta}_2)\cos(\theta_1 + \theta_2) \end{aligned}\right\} \quad (4)$$

where $\dot{\theta}$ represents angular velocity.

In this analysis, the Lagrangian formulation is employed to establish the equation of motion. The mathematical expression for the Lagrangian equation can be articulated according to [24][25][26]:

$$L = KE - PE \quad (5)$$

where *KE* is the kinetic energy, and *PE* represents is the potential energy.

Total kinetic energy of the mechanism can be defined as follows [27][28]:

$$KE = \frac{1}{2}m_1 v_1^2 + \frac{1}{2}m_2 v_2^2 \quad (6)$$

where m_1 and m_2 are the first, second links masses, respectively, v_1, and v_2 represent the linear velocity.

Linear velocity can be expressed in the following formulas:

$$v_1 = \sqrt{\dot{x}_1^2 + \dot{y}_1^2},\ v_2 = \sqrt{\dot{x}_2^2 + \dot{y}_2^2} \quad (7)$$

Consequently, the equation (6) can be reformulated as follows:

$$\begin{aligned} \mathrm{KE} = [0.5(m_1 + m_2)l_1^2 + m_2 l_1 l_2 \cos\theta_2 \\ + 0.5m_2 l_2^2]\dot{\theta}_1^2 + [0.5m_2 l_2^2]\dot{\theta}_2^2 \\ + [m_2 l_1 l_2 \cos\theta_2 + m_2 l_2^2]\dot{\theta}_1\dot{\theta}_2 \end{aligned} \quad (8)$$

The expression for the potential energy at each link can be written as follows:

$$\mathrm{PE} = \sum_{i=1}^{2} \mathrm{m_i\, g\, y_i} \quad (9)$$

where y_i is the vertical height, and g is the gravitational acceleration.

The total potential energy of the two link manipulators is:

$$PE = (m_1 + m_2)gl_1 \sin\theta_1 + m_2 g l_2 \sin(\theta_1 + \theta_2) \quad (10)$$

By substituting Equations (8) and (9) into Equation (5) and simplifying it, it will have the following formula:

$$L = KE - PE \tag{11}$$

$$\begin{aligned} L = {} & [0.5(m_1 + m_2)l_1^2 + m_2 l_1 l_2 \cos\theta_2 \\ & + 0.5m_2 l_2^2]\dot{\theta}_1^2 + [0.5m_2 l_2^2]\dot{\theta}_2^2 \\ & + [m_2 l_1 l_2 \cos\theta_2 + m_2 l_2^2]\dot{\theta}_1\dot{\theta}_2 \\ & - (m_1 + m_2)g l_1 \sin\theta_1 \\ & - m_2 g l_2 \sin(\theta_1 + \theta_2) \end{aligned} \tag{12}$$

$$\left.\frac{d}{dt}\left[\frac{\partial L}{\partial \dot{\theta}_i}\right] - \frac{\partial L}{\partial \theta_i} = \tau_i\right\} \tag{13}$$

where τ is the torque applied to each joint in the system and i=1, 2.

$$\begin{aligned} \frac{\partial L}{\partial \theta_1} = {} & -(m_1 + m_2)g l_1 \cos\theta_1 \\ & - m_2 g l_2 \cos(\theta_1 + \theta_2) \end{aligned} \tag{14}$$

$$\begin{aligned} \frac{\partial L}{\partial \dot{\theta}_1} = {} & [(m_1 + m_2)l_1^2 + m_2 l_2^2 + 2m_2 l_1 l_2 \cos\theta_2]\dot{\theta}_1 \\ & + [m_2 l_1 l_2 \cos\theta_2 + m_2 l_2^2]\dot{\theta}_2 \end{aligned} \tag{15}$$

$$\begin{aligned} \frac{d}{dt}\left[\frac{\partial L}{\partial \dot{\theta}_1}\right] = {} & [(m_1 + m_2)l_1^2 + m_2 l_2^2 \\ & + 2m_2 l_1 l_2 \cos\theta_2 \\ & + 2m_3 l_1 l_2 \cos\theta_2]\ddot{\theta}_1 \\ & + [m_2 l_1 l_2 \cos\theta_2 + m_2 l_2^2]\ddot{\theta}_2 \\ & - [2m_2 l_1 l_2 \sin\theta_2]\dot{\theta}_1\dot{\theta}_2 \\ & - [m_2 l_1 l_2 \sin\theta_2]\dot{\theta}_2^2 \end{aligned} \tag{16}$$

$$\begin{aligned} \frac{\partial L}{\partial \theta_2} = {} & -m_2 l_1 l_2 \sin\theta_2\, \dot{\theta}_1^2 - m_2 l_1 l_2 \sin\theta_2\, \dot{\theta}_1\dot{\theta}_2 \\ & - m_2 g l_2 \cos(\theta_1 + \theta_2) \end{aligned} \tag{17}$$

$$\frac{\partial L}{\partial \dot{\theta}_2} = [m_2 l_1 l_2 \cos\theta_2 + m_2 l_2^2]\dot{\theta}_1 + m_2 l_2^2 \dot{\theta}_2 \tag{18}$$

$$\begin{aligned} \frac{d}{dt}\left[\frac{\partial L}{\partial \dot{\theta}_2}\right] = {} & [m_2 l_1 l_2 \cos\theta_2 + m_2 l_2^2 +]\ddot{\theta}_1 \\ & + [m_2 l_2^2]\ddot{\theta}_2 \\ & - [m_2 l_1 l_2 \sin\theta_2]\dot{\theta}_1\dot{\theta}_2 \end{aligned} \tag{19}$$

Where τ_1 and τ_2 represents the torque at the first, second links respectively, also, θ̈ is the angular acceleration, it can be expressed in the equations below:

$$\begin{aligned} & [(m_1 + m_2)l_1^2 + m_2 l_2^2 + 2m_2 l_1 l_2 \cos\theta_2 \\ & + 2m_3 l_1 l_2 \cos\theta_2]\ddot{\theta}_1 \\ & + [m_2 l_1 l_2 \cos\theta_2 + m_2 l_2^2]\ddot{\theta}_2 \\ & - [2m_2 l_1 l_2 \sin\theta_2]\dot{\theta}_1\dot{\theta}_2 \\ & - [m_2 l_1 l_2 \sin\theta_2]\dot{\theta}_2^2 \\ & + (m_1 + m_2)g l_1 \cos\theta_1 \\ & + m_2 g l_2 \cos(\theta_1 + \theta_2) = \tau_1 \end{aligned} \tag{20}$$

$$\begin{aligned} & [m_2 l_1 l_2 \cos\theta_2 + m_2 l_2^2]\ddot{\theta}_1 + [m_2 l_2^2]\ddot{\theta}_2 \\ & + m_2 l_1 l_2 \sin\theta_2\, \dot{\theta}_1^2 \\ & + m_2 g l_2 \cos(\theta_1 + \theta_2) = \tau_2 \end{aligned} \tag{21}$$

Furthermore, to Equations (20) and (21) it has the capability to represent the overall nonlinear equation of motion governing the movement of the 2-DOF robot in the following manner [30] to [33].

$$M(\theta)\ddot{\theta} + C(\theta, \dot{\theta})\dot{\theta} + G(\theta) = \tau \tag{22}$$

where, M(θ) is the inertia matrix of the links, τ represents the control torque, C (θ, $\dot{\theta}$) $\dot{\theta}$ is the Coriolis force, and $G(\theta)$ signifies gravitational force.

$$M(\theta) = \begin{bmatrix} M_{11} & M_{12} \\ M_{21} & M_{22} \end{bmatrix} \tag{23}$$

Where

$$\begin{aligned} M_{11} = {} & (m_1 + m_2)l_1^2 + m_2 l_2^2 + 2m_2 l_1 l_2 \cos\theta_2 \\ & + 2m_3 l_1 l_2 \cos\theta_2 \end{aligned}$$

$$M_{12} = m_2 l_1 l_2 \cos\theta_2 + m_2 l_2^2$$

$$M_{21} = m_2 l_1 l_2 \cos\theta_2 + m_2 l_2^2$$

$$M_{22} = m_2 l_2^2$$

$$C(\theta, \dot{\theta}) = \begin{bmatrix} C_1 \\ C_2 \end{bmatrix} \tag{24}$$

Where

$$C_1 = -[2m_2 l_1 l_2 \sin\theta_2]\dot{\theta}_1\dot{\theta}_2 - [m_2 l_1 l_2 \sin\theta_2]\dot{\theta}_2^2$$

$$C_2 = m_2 l_1 l_2 \sin\theta_2\, \dot{\theta}_1^2$$

$$G(\theta, \dot{\theta}) = \begin{bmatrix} G_1 \\ G_2 \end{bmatrix} \tag{25}$$

Where

$$G_1 = (m_1 + m_2)g l_1 \cos\theta_1 + m_2 g l_2 \cos(\theta_1 + \theta_2)$$

$$G_2 = m_2 g l_2 \cos(\theta_1 + \theta_2)$$

$$\begin{bmatrix} M_{11} & M_{12} \\ M_{21} & M_{22} \end{bmatrix}\begin{bmatrix} \ddot{\theta}_1 \\ \ddot{\theta}_2 \end{bmatrix} + \begin{bmatrix} C_1 \\ C_2 \end{bmatrix}\begin{bmatrix} \dot{\theta}_1 \\ \dot{\theta}_2 \end{bmatrix} + \begin{bmatrix} G_1 \\ G_2 \end{bmatrix} = \begin{bmatrix} \tau_1 \\ \tau_2 \end{bmatrix} \tag{26}$$

$$\tau_1 = \mathrm{M}_{11}\ddot{\theta}_1 + \mathrm{M}_{12}\ddot{\theta}_2 + \mathrm{C}_1\dot{\theta}_1 + G_1 \tag{27}$$

$$\tau_2 = \mathrm{M}_{21}\ddot{\theta}_1 + \mathrm{M}_{22}\ddot{\theta}_2 + \mathrm{C}_2\dot{\theta}_2 + G_2 \tag{28}$$

$$\ddot{\theta}_1, \ddot{\theta}_2, and\ \ddot{\theta}_3\ are:$$

$$\ddot{\theta}_1 = \frac{1}{M_{11}}\left(\tau_1 - M_{12}\ddot{\theta}_2 - C_1\dot{\theta}_1 - G_1\right) \tag{29}$$

$$\ddot{\theta}_2 = \frac{1}{M_{22}}\left(\tau_2 - M_{21}\ddot{\theta}_1 - C_2\dot{\theta}_2 - G_2\right) \tag{30}$$

Variable in State Space:

A state variable in the state equation can be used to represent the following [34][35].

$x_1 = \theta_1 \quad x_3 = \theta_2$ (Angular position of the links)

$x_2 = \dot{\theta}_1 \quad x_4 = \dot{\theta}_2$ (Angular velocity of the links)

Equations (31) to (34) highlights the highly nonlinear dynamics of the 2-DOF robot. By selecting appropriate state variables in the state equation, it can be expressed as follows:

$$\dot{x_1} = \dot{\theta}_1 = x_2 \tag{31}$$

$$\dot{x_2} = \ddot{\theta}_1 = \frac{1}{M_{11}}\left(\tau_1 - M_{12}\ddot{\theta}_2 - C_1\dot{\theta}_1 - G_1\right) \tag{32}$$

$$\dot{x_3} = \dot{\theta}_2 = x_4 \tag{33}$$

$$\dot{x_4} = \ddot{\theta}_2 = \frac{1}{M_{22}}\left(\tau_2 - M_{21}\ddot{\theta}_1 - C_2\dot{\theta}_2 - G_2\right) \tag{34}$$

$u_1 = \tau_1$ (First link actuator's torque)
$u_2 = \tau_2$ (Second link actuator's torque)

III. CONTROL DESIGN

A. Classic Synergetic Control Algorithm (CSC)

Current control theory struggles to adequately address the complexity of intricate macro-systems, characterized by multi-dimensional, nonlinear dynamics and interconnected subsystems exchanging information, matter, and power, making it challenging to identify common control laws for system synthesis. Classic Synergetic Control (CSC) is a comprehensive approach designed to manage nonlinear systems by integrating multiple control mechanisms to ensure stability and resilience despite uncertainties and nonlinearities, offering a solution to the challenges posed by inherently unstable systems [36].

1) Synergetic control theory synthesis

The system of nonlinear dynamics depicted in Equation (35). The first step in creating a synergistic controller is to define a macro-variable that takes into account the specifications and control constraints given in Equation (36) [37][38].

$$\dot{x} = f(x, u, t) \tag{35}$$

In this context, *x* represents the state vector of the system, the control vector is denoted by u and t is the time.

$$\sigma(t) = \sigma(x, t) \tag{36}$$

$\sigma(t)$ represents the macro-variable, while the objective function (*x, t*) is specified to undergo development within the selected domain as outlined in Equation (37) [39].

$$\sigma(x, t) = 0 \tag{37}$$

The control objective, settling time, and control constraints are some of the considerations the designer makes when choosing the macro-variable's characteristics. The macro-variable vector's size does not exceed the number of control channels [40]. It can be a linear combination of state variables that are made to evolve in a desired manner as indicated by a constraint selected by the designer, as demonstrated in Equation (38).

$$T\dot{\sigma(t)} + \sigma(t) = 0 \tag{38}$$

where the control parameter T indicates the converging ratio of $\sigma(t)$to manifold with $\dot{\sigma(t)}$where T is greater than zero [41][42].

By selecting appropriate macro-variables, the synergetic control system can achieve global stability, resilience to parameter changes, and efficiency without the disadvantages of chattering [43].

2) Classic Synergetic Controller Design (CSC)

This subsection presents a control strategy for tracking angular position. The control is designed using the classic synergetic control approach [44] to develop the (CSC) algorithm for system in the absence of external disturbances, adhere to the steps outlined [5].

The first step in the design is to define the error e_1 is the difference between the desired angle position ($x_{1d} = \theta_{1d}$) and the actual angle position ($x_1 = \theta_1$).

$$e_1 = x_1 - x_{1d} \tag{39}$$

$$e_2 = x_3 - x_{3d} \tag{40}$$

e_2 is the difference between the desired angle position ($x_{2d} = \theta_{2d}$) and the actual angle position ($x_2 = \theta_2$).

By calculating the first and second derivatives, one can obtain the desired outcome.

$$\dot{e_1} = \dot{x_1} - \dot{x_{1d}} = x_2 - \dot{x_{1d}} \tag{41}$$

$$\dot{e_2} = \dot{x_3} - \dot{x_{3d}} = x_4 - \dot{x_{3d}} \tag{42}$$

$$\ddot{e_1} = \dot{x_2} - \ddot{x_{1d}} = \frac{1}{y}(M_{22}u_1 - M_{12}u_2 + M_{12}C_2 + M_{12}G_2 - M_{22}C_1 - M_{22}G_1) - \ddot{x_{1d}} \tag{43}$$

$$\ddot{e_2} = \dot{x_3} - \ddot{x_{3d}} = \frac{1}{y}(M_{11}u_2 - M_{21}u_1 + M_{21}C_1 + M_{21}G_1 - M_{11}C_2 - M_{11}G_2) - \ddot{x_{3d}} \tag{44}$$

where,
$y = M_{11}M_{22} - M_{12}M_{21}$

The dynamic equation of the Marco variable σ is described as

$$\sigma_1 = ce_1 + \dot{e_1} \tag{45}$$

$$\sigma_2 = ce_2 + \dot{e_2} \tag{46}$$

In this context, the scalar design for synergetic control is denoted as c, where c is a positive value.

$$\dot{\sigma_1} = c\dot{e_1} + \ddot{e_1} \tag{47}$$

$$\dot{\sigma_2} = c\dot{e_2} + \ddot{e_2} \tag{48}$$

The symbol $\dot{\sigma_1}$ and $\dot{\sigma_2}$ denotes the manifold equation variable as defined within the context.

$$T\dot{\sigma_1} + \sigma_1 = 0 \tag{49}$$

$$T\dot{\sigma_2} + \sigma_2 = 0 \tag{50}$$

where T is greater than 0, is the converging ratio of σ to manifold with $\dot{\sigma}$.

By substituting Equations (47) and (48) into Equations (49) and (50), to obtain:

$$T(c\dot{e_1} + \ddot{e_1}) + \sigma_1 = 0 \tag{51}$$

$$T(c\dot{e_2} + \ddot{e_2}) + \sigma_2 = 0 \tag{52}$$

Additionally, by utilizing Equations (47) to (51), one can derive:

$$T\left(c\dot{e}_1 + \left(\frac{1}{y}(M_{22}u_1 - M_{12}u_2 + M_{12}C_2 + M_{12}G_2 - M_{22}C_1 - M_{22}G_1) - \ddot{x_{1d}}\right)\right) + \sigma_1 = 0 \quad (53)$$

$$T\left(c\dot{e}_2 + \frac{1}{y}(M_{11}u_2 - M_{21}u_1 + M_{21}C_1 + M_{21}G_1 - M_{11}C_2 - M_{11}G_2) - \ddot{x_{2d}}\right) + \sigma_2 = 0 \quad (54)$$

The synergetic control law for a robot arm can be derived from Equations (53) and (54), as demonstrated below:

$$u_1 = M_{11}\left(-c\dot{e}_1 + \ddot{x_{1d}} - \frac{\sigma_1}{T}\right) + M_{12}\dot{x_4} + C_1x_2 + G_1 \quad (55)$$

$$u_2 = M_{21}\dot{x_2} + M_{22}\left(-c\dot{e}_2 + \ddot{x_{3d}} - \frac{\sigma_2}{T}\right) + C_2x_4 + G_2 \quad (56)$$

Fig. 3 illustrates the schematic representation of the synergetic control design for a robot arm.

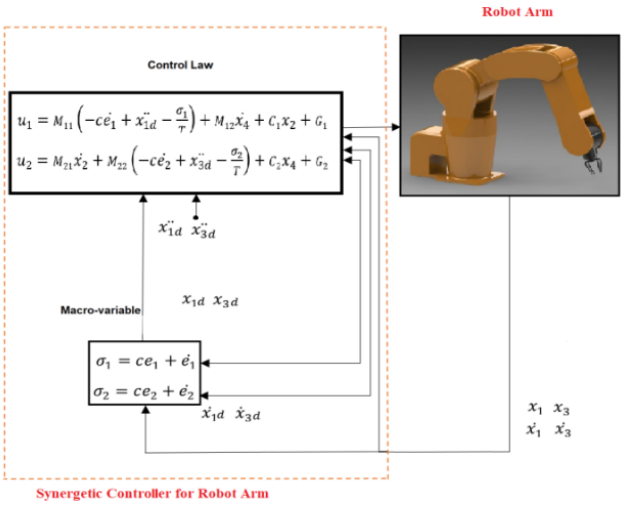

Fig. 3. Schematic diagram of Classic synergetic control

B. Adaptive Synergetic Control Algorithm (ASC)

ASC represents an enhanced iteration of the CSC approach. The certainty equivalence adaptive control method is among various contemporary adaptive strategies that rely on adaptive laws to estimate unidentified parameters in order to accurately reflect the true values of these parameters. This process ultimately contributes to maintaining the stability of the adaptive controlled system [45] was used Lyapunov stability to extract laws [46][47].

1) Adaptive Synergetic Control Theory Synthesis

The ASC approach has been proposed to address uncertainties in a system's physical parameters and reduce the negative effects of disturbances on tracking performance. This method focuses on developing adaptive laws to accurately estimate these uncertain parameters, thereby ensuring the stability of the adaptive control system [48]. Consider the Lyapunov candidate function as.

$$V = \frac{1}{2}\sigma^2 + \frac{1}{2}\gamma^{-1}\tilde{F_j}^2 \quad (57)$$

The uncertainty will be debate for disturbance where j number of disturbances. In the given context, F represents the estimated error disturbance and γ is the adaptation gains.

The estimated error disturbance can be represented by the following formula:

$$\tilde{F_j} = F_j - \hat{F_j} \quad (58)$$

F_1 represents an unidentified external disturbance and $\hat{F_j}$ the estimation of disturbance F_j. derivative V is express as follow:

$$\dot{V} = \sigma\dot{\sigma} - \gamma^{-1}\tilde{F_j}\dot{\hat{F}_j} \quad (59)$$

To maintain the negative definiteness of the $\dot{V}$ function, the adaptive laws will be as follows:

$$\dot{\hat{F}_j} = -\gamma^{-1}\sigma(c\dot{e} + \ddot{e}) \quad (60)$$

According to Lyapunov stability theory, it is necessary for the time derivative of a Lyapunov function, denoted as V, to exhibit negative definiteness [49].

The proposed Adaptive Synergetic Control approach ensures the system's asymptotic stability, even when encountering uncertainties in the system's parameters [50].

2) Adaptive Synergetic Controller Design (ASC)

This section presents an adaptive control strategy for dealing with uncertainty that employs a synergetic method. First, the traditional synergetic control approach is outlined, then the adaptive synergetic control design is applied to create control and adaptive laws to deal with variations in the system's coefficients [51]. To develop the ASC algorithm for a 2-DoF robot manipulator, adhere to the outlined procedures [48].

$$\dot{x_2} = \ddot{\theta_1} = \frac{1}{y}(M_{22}u_1 - M_{12}u_2 + M_{12}C_2 + M_{12}G_2 - M_{22}C_1 - M_{22}G_1 - M_{22}F_1) \quad (61)$$

$$\dot{x_4} = \ddot{\theta_2} = \frac{1}{y}(M_{11}u_2 - M_{21}u_1 + M_{21}C_1 + M_{21}G_1 - M_{11}C_2 - M_{11}G_2 - M_{11}F_2) \quad (62)$$

F_1 is intended to represent an unidentified external disruption.

$$\dot{V_1} = \frac{1}{2}(\sigma_1)^2 + \frac{1}{2}\gamma^{-1}\left(\tilde{F_1}\right)^2 \quad (63)$$

In this context, $\tilde{F_1}$denotes the estimated error disturbance.

$$\tilde{F_1} = F_1 - \hat{F_1} \quad (64)$$

$\hat{F_1}$ represents the estimation of disturbance $F_1$and Gamma represents the adaptation gain.

By finding the derivative of Equation (63) with respect to time, it was obtained

$$\dot{V_1} = \sigma_1\dot{\sigma_1} - \gamma^{-1}\tilde{F_1}\dot{\hat{F}_1} \quad (65)$$

By replacing the expression from Equation (47) into Equation (65), the result is obtained.

$$\dot{V_1} = \sigma_1(c\dot{e_1} + \ddot{e_1}) - \gamma^{-1}\tilde{F_1}\dot{\hat{F}_1} \quad (66)$$

By substituting the expression from Equation (43) into Equation (66), was obtained.

$$\dot{V}_1 = \sigma_1\Big(c\dot{e}_1 + \frac{1}{y}(M_{22}u_1 - M_{12}u_2 + M_{12}C_2 + M_{12}G_2 - M_{22}C_1 - M_{22}G_1 - M_{22}F_1) - \ddot{x_{1d}}\Big) - \gamma^{-1}\tilde{F}_1\dot{\hat{F}}_1 \quad (67)$$

$$\dot{V}_1 = \sigma_1\Big(c\dot{e}_1 + \frac{1}{y}\Big(M_{22}\Big(-M_{11}c\dot{e}_1 + M_{11}\ddot{x_{1d}} - \frac{M_{11}\sigma_1}{T} - M_{12}c\dot{e}_2 + M_{12}\ddot{x_{3d}} - \frac{M_{12}\sigma_2}{T} + C_1 + G_1 + \hat{F}_1\Big) - M_{12}\Big(-M_{21}c\dot{e}_1 + M_{21}\ddot{x_{1d}} - \frac{M_{21}\sigma_1}{T} - M_{22}c\dot{e}_2 + M_{22}\ddot{x_{3d}} - \frac{M_{22}\sigma_2}{T} + C_2 + G_2\Big) + M_{12}C_2 + M_{12}G_2 - M_{22}C_1 - M_{22}G_1 - M_{22}F_1\Big) - \ddot{x_{1d}}\Big) - \gamma^{-1}\tilde{F}_1\dot{\hat{F}}_1 \quad (68)$$

$$\dot{V}_1 = -\frac{{\sigma_1}^2}{T} + \frac{M_{22}\sigma_1}{y}(\hat{F}_1 - F_1) - \gamma^{-1}\tilde{F}_1\dot{\hat{F}}_1 \quad (69)$$

$$\dot{V}_1 = -\frac{{\sigma_1}^2}{T} - \frac{M_{22}\sigma_1}{y}\tilde{F}_1 - \gamma^{-1}\tilde{F}_1\dot{\hat{F}}_1 \quad (70)$$

$$\dot{V}_1 = -\frac{{\sigma_1}^2}{T} - \Big(\frac{M_{22}\sigma_1}{y} + \gamma^{-1}\dot{\hat{F}}_1\Big)\tilde{F}_1 \quad (71)$$

To ensure that V is less than or equal to zero, the second term has been adjusted to zero.

$$\Big(\frac{M_{22}\sigma_1}{y} + \gamma^{-1}\dot{\hat{F}}_1\Big) = 0 \quad (72)$$

As a result, the following laws of adaptation can be inferred:

$$\dot{\hat{F}}_1 = \frac{-M_{22}\sigma_1}{y}\gamma^{-1} \quad (73)$$

Similarly, in the context of variable $\dot{V}_2$

$$\dot{V}_2 = \frac{1}{2}(\sigma_2)^2 + \frac{1}{2}\gamma^{-1}\big(\widetilde{F_2}\big)^2 \quad (74)$$

$$\widetilde{F_2} = F_2 - \widehat{F_2} \quad (75)$$

$$\dot{V}_2 = \sigma_2\dot{\sigma}_2 - \gamma^{-1}\widetilde{F_2}\dot{\widehat{F_2}} \quad (76)$$

$$\dot{V}_2 = \sigma_2(c\dot{e}_2 + \ddot{e}_2) - \gamma^{-1}\widetilde{F_2}\dot{\widehat{F_2}} \quad (77)$$

$$\dot{V}_2 = \sigma_2\Big(c\dot{e}_2 + \frac{1}{y}(M_{11}u_2 - M_{21}u_1 + M_{21}C_1 + M_{21}G_1 - M_{11}C_2 - M_{11}G_2 - M_{11}F_2) - \ddot{x_{3d}}\Big) - \gamma^{-1}\widetilde{F_2}\dot{\widehat{F_2}} \quad (78)$$

$$\dot{V}_2 = \sigma_2\Big(c\dot{e}_2 + \frac{1}{y}\Big(M_{11}\Big(-M_{21}c\dot{e}_1 + M_{21}\ddot{x_{1d}} - \frac{M_{21}\sigma_1}{T} - M_{22}c\dot{e}_2 + M_{22}\ddot{x_{3d}} - \frac{M_{22}\sigma_2}{T} + C_2 + G_2 + \widehat{F_2}\Big) - M_{21}\Big(-M_{11}c\dot{e}_1 + M_{11}\ddot{x_{1d}} - \frac{M_{11}\sigma_1}{T} - M_{12}c\dot{e}_2 + M_{12}\ddot{x_{3d}} - \frac{M_{12}\sigma_2}{T} + C_1 + G_1\Big) + M_{21}C_1 + M_{21}G_1 - M_{11}C_2 - M_{11}G_2 - M_{11}F_2\Big) - \ddot{x_{3d}}\Big) - \gamma^{-1}\widetilde{F_2}\dot{\widehat{F_2}} \quad (79)$$

$$\dot{V}_2 = -\frac{{\sigma_2}^2}{T} - \frac{M_{11}\sigma_2}{y}(F_2 - \widehat{F_2}) - \gamma^{-1}\widetilde{F_2}\dot{\widehat{F_2}} \quad (80)$$

$$\dot{V}_2 = -\frac{{\sigma_2}^2}{T} - \frac{M_{11}\sigma_2}{y}\widetilde{F_2} - \gamma^{-1}\widetilde{F_2}\dot{\widehat{F_2}} \quad (81)$$

$$\dot{V}_2 = -\frac{{\sigma_2}^2}{T} - \Big(\frac{M_{11}\sigma_2}{y} + \gamma^{-1}\dot{\widehat{F_2}}\Big)\widetilde{F_2} \quad (82)$$

In order to guarantee that the value of V remains at or below zero, the second term has been modified to zero.

$$\Big(\frac{M_{11}\sigma_2}{y} + \gamma^{-1}\dot{\widehat{F_2}}\Big) = 0 \quad (83)$$

Consequently, the subsequent principles of adaptation can be deduced.

$$\dot{\widehat{F_2}} = \frac{-M_{11}\sigma_2}{y}\gamma^{-1} \quad (84)$$

The proposed adaptive synergetic control approach is illustrated in Fig. 4 as a schematic diagram.

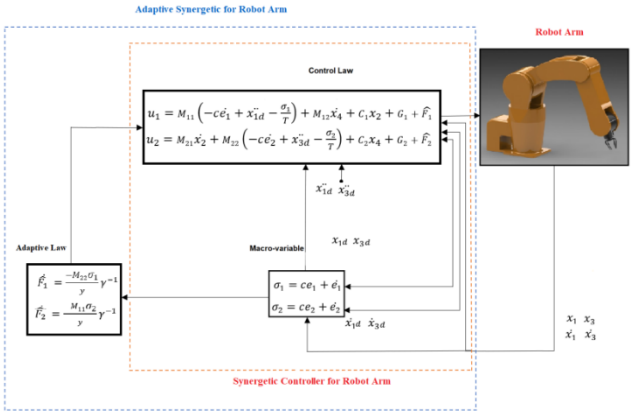

Fig. 4. Schematic diagram of Adaptive synergetic control

IV. SIMULATION RESULTS AND DISCUSSION

In this work, MATLAB/SIMULINK was used to create a model and simulate the system. The control algorithms and system model are coded using m-functions. The principal body of the system under control was fabricated and designed inside the SIMULINK setting. The design parameter values for the CSC and ASC are given in Table I, and configuration options for the 2-DoF robot system. Table II illustrates non-optimal parameter settings such as (the scalar design and

converging ratio were determined through a process of trial and error.

TABLE I. DESIGN PARAMETERS OF CSC AND ASC A VALUE FOR A 2-DOF ROBOT [52]

Parameter	Definition	Value	Units
l_1	Length of link 1	0.040	m
l_2	Length of link 2	0.025	m
m_1	Mass of link 1	0.009	Kg
m_2	Mass of link 2	0.005	Kg
θ_{1d}	Desired angle position for link1	$\frac{\pi}{2}[1-e^{(-5t)}(5t+1)]$	rad
θ_{2d}	Desired angle position for link2	$\frac{\pi}{2}[1-e^{(-5t)}(5t+1)]$	rad
g	Gravitational constant	9.81	m/s^2

TABLE II. THE DESIGN PARAMETERS OF SC AND ASC VALUES FOR A 2-DOF ROBOT

Parameters	Definition	Design Parameters	Controller
c	scalar design	8	CSC
T	converging ratio	0.0003	
c	scalar design	5	ASC
T	converging ratio	0.000001	
γ_1	adaptation gain	0.00000001	
γ_2	adaptation gain	0.00000001	

Fig. 4 demonstrates the arrangement of links for the model controlled in CSC.

A. Validation and Verification

To validate the results of the methodology used in this study, a comparison will be made with the reference [53], In terms of dynamic analysis, this study is closer to the system used in this work, but it takes a different approach, using CSMC and ASMC on the 2-link robot. As a result, the comparison will be performed to ensure the accuracy of the algorithms used in this study.

Fig. 5 and Fig. 6 show the angular position results compared to the reference [53]. From Fig. 5, it is clear that the classical synergistic control proved its superior efficiency and robustness over CSMC, as a significant improvement in tracking the angular position smoothly and in less time than the CSMC algorithm was observed by 76.9%.

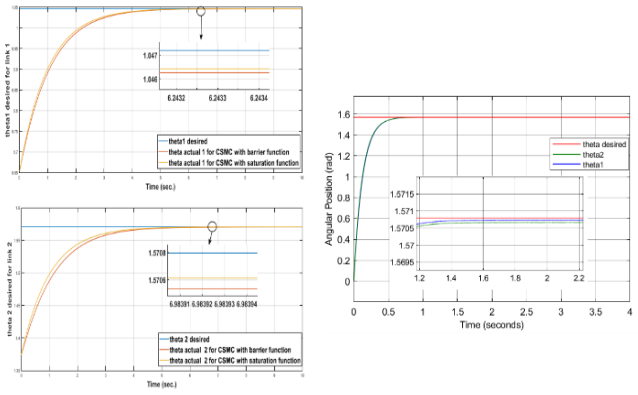

a. CSMC b. CSC

Fig. 5. Tracking performance between the desired and existing position

Fig. 6 shows that the adaptive synergistic control has proven to be efficient and superior to ASMC, with a significant improvement of 63% in smooth, without chatter, and timely angular position tracking over the ASMC algorithm.

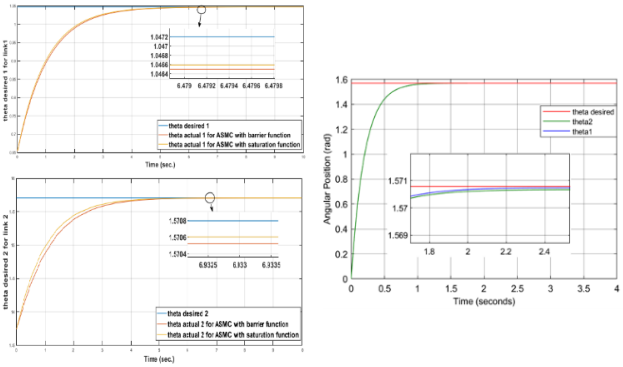

a. ASMC b. CSC

Fig. 6. Tracking performance between the desired and existing position

It was observed that the tracking response, achieving the desired position, occurred within a maximum of 1.5 seconds for CSC, with visible oscillations as shown in Fig. 7. Furthermore, the time taken to connect to the desired position is favorable compared to earlier research, yet the drawback lies in the occurrence of chattering.

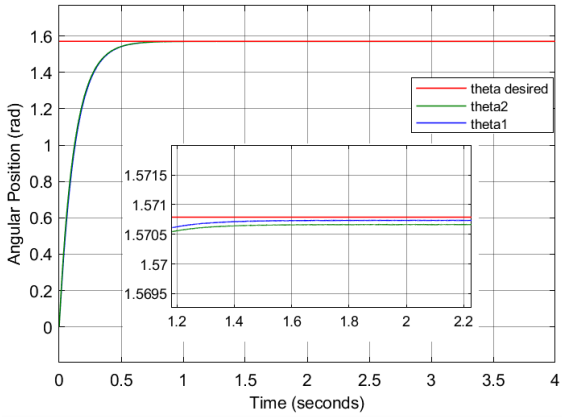

Fig. 7. Tracking performance between the desired and existing position of CSC algorithm

Fig. 8 illustrates the arrangement of the links for the model under ASC control. The study revealed that the time taken for the tracking performance to reach the desired position was within 2.4 seconds when utilizing ASC.

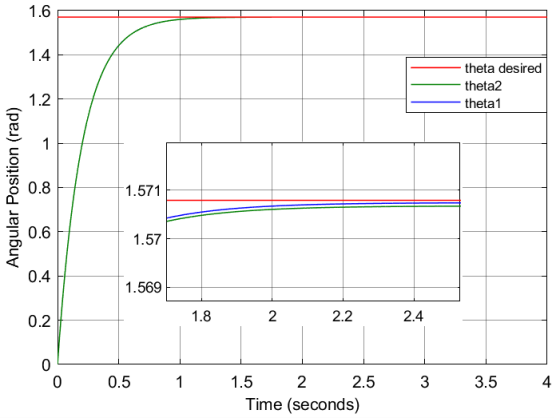

Fig. 8. Tracking performance between the desired and existing position of ASC

In Fig. 9, the adaptive synergistic controller demonstrates greater efficiency and flexibility compared to the Synergy Controller in terms of performance. Through Fig. 9, it was found that the tracking time using CSC is less than the tracking time using ASC. However, there is a clear presence of chattering in CSC, while using ASC eliminates all of the chattering effects in the CSC through continuously adjusting the control parameters in reaction to the behavior of the system. This dynamic adjustment helps in reducing the chattering effect and stabilizing the system [54,55,56]. The Root Mean Square (RMS) for CSC was found to be 1.57 rad, where ASC did not RMS. The improvement rate in ASC compared to CSC was 100%.

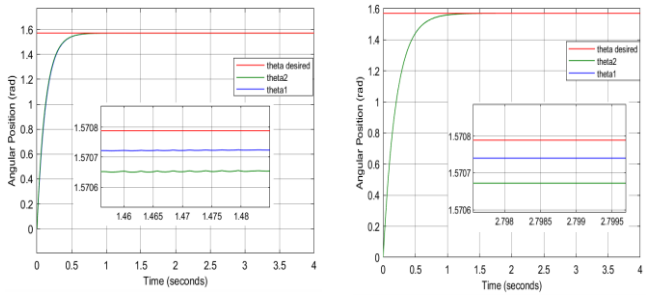

a. CSC b. ASC

Fig. 9. Comparison of tracking performance between the desired and existing position for CSC and ASC

Fig. 10 illustrates the control action in conventional synergistic control, where the initial control action reaches a peak of 1.1988 N/m, followed by a second control action peaking at 0.2606 N/m, and both actions stabilize simultaneously after 0.4 seconds.

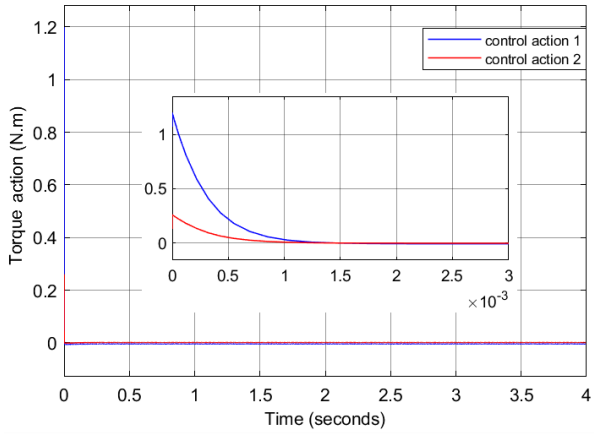

Fig. 10. First and second control of action response using CSC

In Fig. 11, the shown the control procedure for adaptive synergistic control. The initial control action reaches its maximum at 224.995 N/m units. Subsequently, a second control action peaks at a of 49 N/m, and both actions stabilize simultaneously after 0.8×10^{-5} sec seconds.

Obviously, ASC achieves higher control procedures than CSC. This indicates that the ASC uses more energy than the CSC. This is the price paid by the ASC for an enhanced dynamic response.

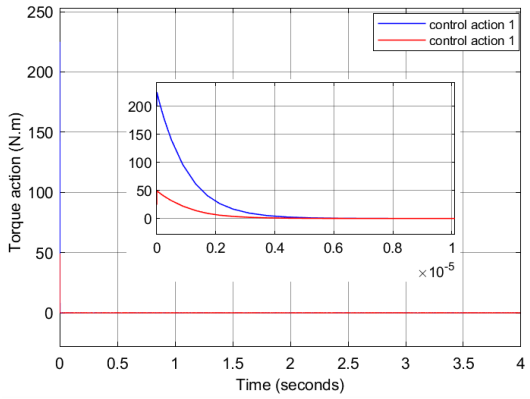

Fig. 11. First and second control of action response using ASC

Fig. 12 and Fig. 13 shows the angular velocity of CSC and ASC. The initial angular velocity reaches a maximum of 12.1 rad/s, while the subsequent angular velocity peaks at 13.3 rad/s. Both velocities reach a stable state simultaneously after 1 seconds at point C. For ASC, both the first and second angular velocities peak at 7.85 stabilizing around 1.4 seconds.

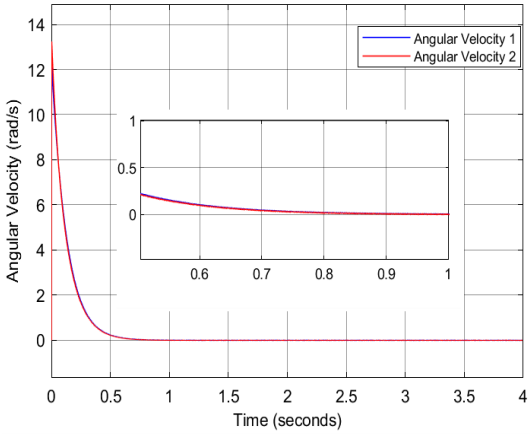

Fig. 12. Angular velocity response for using CSC

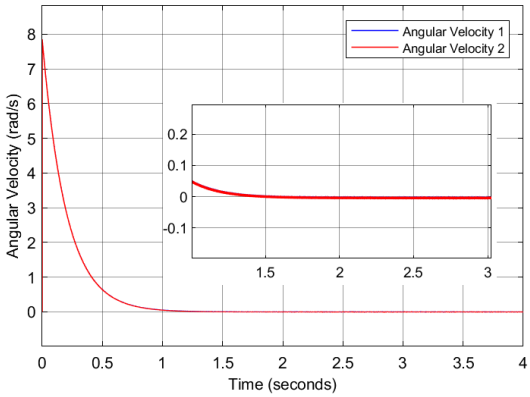

Fig. 13. Angular velocity response for using ASC

The simulation results can be seen in Fig. 14 and Fig. 15 for the tracking error between the CSC and ASC, the velocity error behavior for CSC and ASC are shown in Fig. 16 and Fig. 17. Is found that the CSC peak velocity error response is higher than ASC peak velocity error response Because the system is unable to adapt quickly to dynamic changes, resulting in increased velocity error, the velocity error response in ASC is slower because the system can adjust its

parameters instantly based on changes, reducing errors and improving accuracy and stability [57].

The system can be describing was global asymptotic stability to the by the convergence the of angular position to each link to the desired position. These two controllers (CSC and ASC) can make the system asymptotically stable by forcing the error and the derivative of the error to reach zero at a good time in the final trajectory, resulting in precise tracking of the movement of the 2-DoF robot [58].

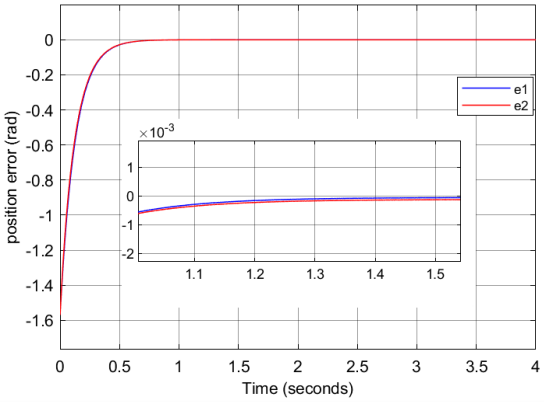

Fig. 14. Position error response for using CSC

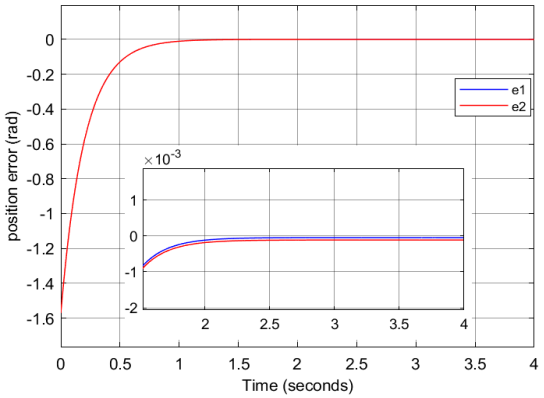

Fig. 15. Position error response for using ASC

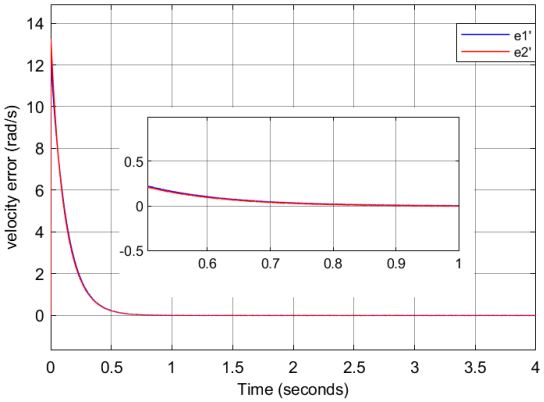

Fig. 16. Velocity error response for using CSC

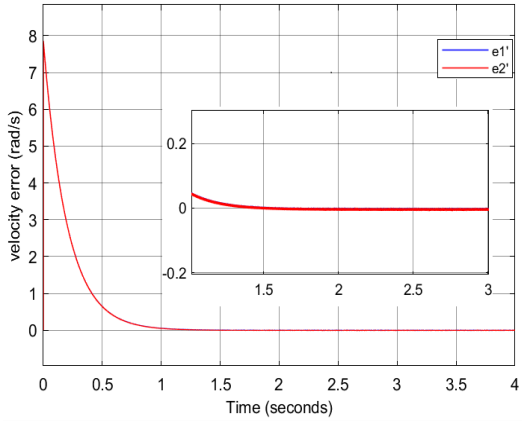

Fig. 17. Velocity error response for using ASC

B. Uncertainty in the System

To verify the system's response and evaluate the effectiveness of the designed control units in this study, uncertainty will be introduced into the proposed model. Additionally, trial and error will be used to adjust the load mass (m) for the 2-DoF robot system controlled by 25%, 50%, 70%, and 90% [59]. These values have been chosen because the load mass is a critical parameter, as indicated in Table III.

Table 3: The design parameters of CSC and ASC a value for a 2-DoF robot with of uncertainty

Parameter	Definition	Value (Kg)	uncertainty
m_1	Mass of link 1	0.01125	25%
m_2	Mass of link 2	0.00625	
m_1	Mass of link 1	0.0135	50%
m_2	Mass of link 2	0.0075	
m_1	Mass of link 1	0.0153	70%
m_2	Mass of link 2	0.0085	
m_1	Mass of link 1	0.0171	90%
m_2	Mass of link 2	0.0095	

The variation in load masses has a significant impact on the controller's performance, including response accuracy [60]. If the mass is greater than expected, the controller may need to exert more effort to achieve the same response, affecting accuracy and may making the system take longer to reach a steady state. This can have an impact on performance when a quick response is required. Additionally, it affects the system's stability. Unexpected load masses may cause oscillations in the system or possibly instability if the controller isn't made to adjust for mass changes. It may have an impact on how the system reacts to perturbations and changes. Thorough analysis is necessary to guarantee the system's stability in various scenarios.

Fig. 18, Fig. 19, and Fig. 20 are expected to undergo slight parameter adjustments through the CSC algorithm in this process, while Fig. 21 to Fig. 23 demonstrate their impact in the ASC algorithm.

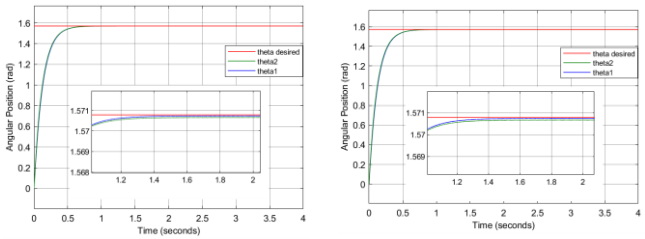

a.25 % b.50 %

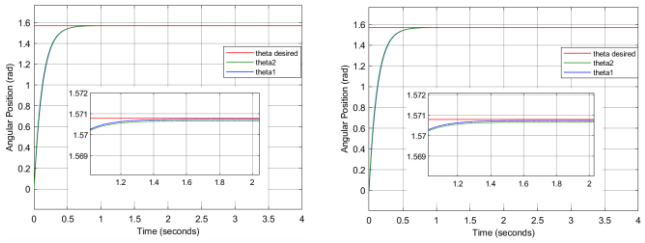

e.70 % f.90%

Fig. 18. Angular position function phase plot at uncertainty of CSC

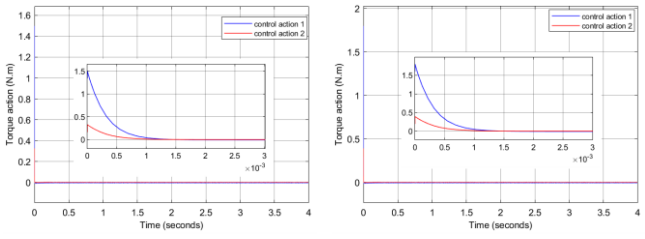

a.25 % b.50 %

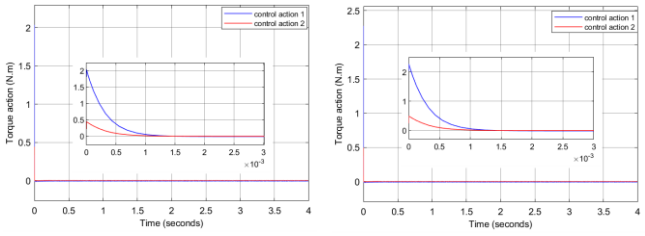

e.70 % f.90%

Fig. 19. Control action function phase plot at uncertainty of CSC

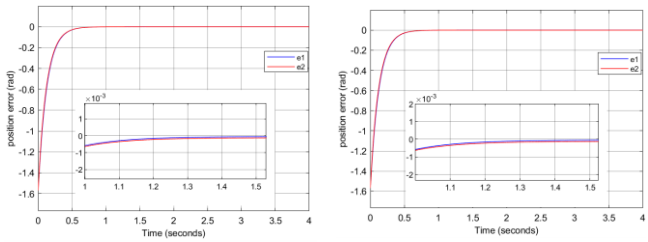

a.25 % b.50 %

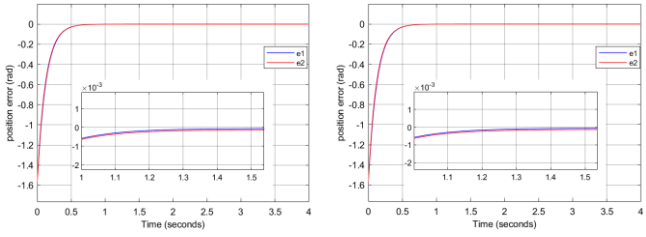

e.70 % f.90%

Fig. 20. Position error function phase plot at uncertainty of CSC

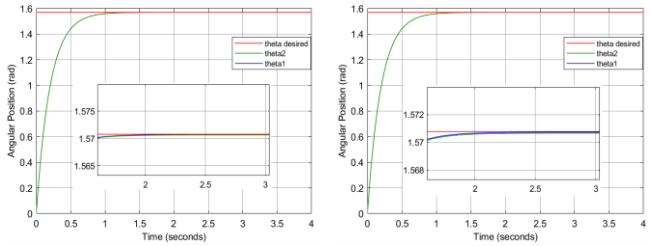

a.25 % b.50 %

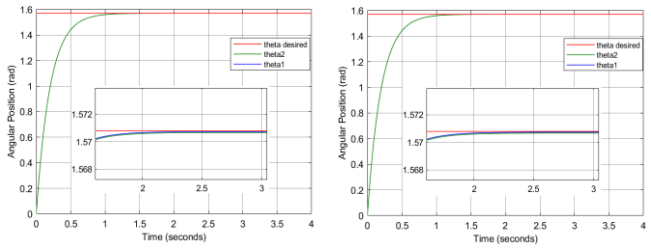

c.70 % e.90%

Fig. 21. Angular position function phase plot at uncertainty of ASC

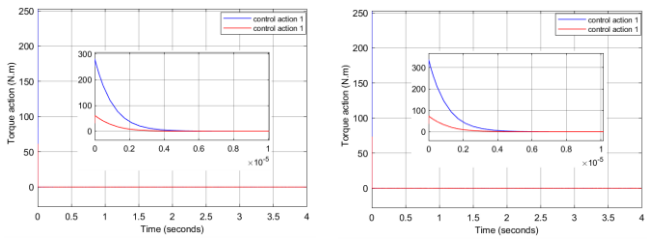

a.25 % b.50 %

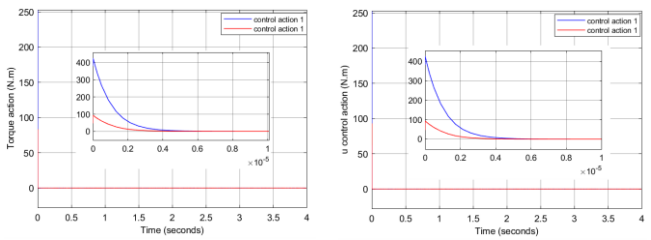

c.70 % e.90%

Fig. 22. Control action function phase plot at uncertainty of ASC

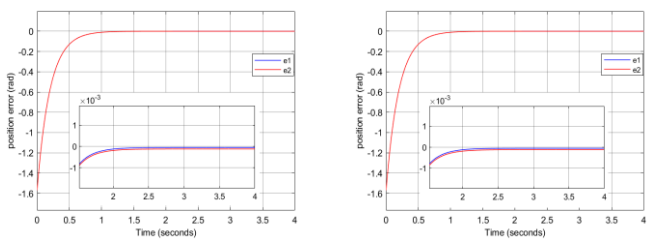

a.25 % d.50 %

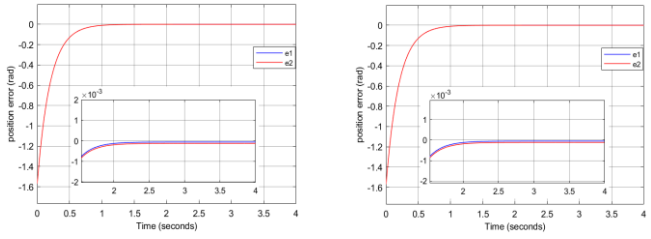

e.70 % f.90%

Fig. 23. Position error function phase plot at uncertainty of ASC

Based on the above illustrations, it can be inferred that the introduction of uncertainty has no significant effect on the operating speed or stability duration of the system, thus verifying the efficiency of the CSC and ASC controller. Therefore, understanding the effect of changing load masses on performance and stability is important for designing reliable and adaptable control systems in practical applications. The masses may not always be constant. Therefore, the CSC and ASC controller are able to adapt to changes in mass to ensure consistent performance. The system has been tested with a range of load masses to ensure that the controller performs well under all possible conditions. It is able to handle a wide range of conditions without loss of stability or performance.

V. CONCLUSIONS

In this study, an adaptive synergetic control (ASC) design was created for a 2-DoF robot system to remediate model uncertainty and external disturbances. The effectiveness of this design was confirmed by numerical simulations that included variations (25%, 50%, 70%, and 90%) in parameter values. The focus of the design was on controlling the angular position of the system. The simulation revealed that ASC is a highly promising and robust control technology, capable of accurately guiding the system to its desired position without oscillations, even under large parameter variations. Future work in this research will concentrate on finding the values of the CSC and ASC control parameters using one of the optimization methods. In addition to the potential for scaling to more complex robotic systems, and the challenges of real-world implementation.

In conclusion, ASC has demonstrated itself as a reliable and effective strategy for enhancing the performance and robustness of 2-DoF robot systems, paving the way for advancements in precision control technology.

REFERENCES

[1] R. M. Murray, Z. Li, and S. S. Sastry. *A mathematical introduction to robotic manipulation*. CRC press, 2017.

[2] N. Elkhateeb and R. I. Badr, "Novel PID tracking controller for 2DOF robotic manipulator system based on artificial bee colony algorithm," *The Scientific Journal of Riga Technical University-Electrical, Control and Communication Engineering*, vol. 13, pp. 55-62, 2017.

[3] S. S. Ray. *Numerical analysis with algorithms and programming*. Chapman and Hall/CRC, 2018.

[4] S. N. Essiane, J. T. Bissé, and M. J. P. Pesdjock, "Simple adaptive synergetic control scheme based on the mit rule of the dc motor," *European Journal of Applied Physics*, vol. 2, no. 6, 2020, doi: 10.24018/ejphysics.2020.2.6.30.4.

[5] A. N. Popov, "Synergetic synthesis of tracking control systems," in *IOP Conference Series: Materials Science and Engineering*, vol. 1029, no. 1, p. 012032, 2021, doi: 10.1088/1757-899X/1029/1/012032.

[6] M. Baccouch and S. Dodds, "A two-link robot manipulator: Simulation and control design," *International Journal of Robotic Engineering*, vol. 5, no. 12, 2020, doi: 10.35840/2631-5106/4128.

[7] J. Jalani, N. Mahyuddin, G. Herrmann, and C. Melhuish, "Active robot hand compliance using operational space and Integral Sliding Mode Control," in *2013 IEEE/ASME International Conference on Advanced Intelligent Mechatronics*, pp. 1749-1754, 2013.

[8] K. Lochan and B. K. Roy, "Control of two-link 2-DOF robot manipulator using fuzzy logic techniques: a review," in *Proceedings of Fourth International Conference on Soft Computing for Problem Solving: SocProS 2014*, vol. 1, pp. 499-511, 2014.

[9] G. Herrmann, J. Jalani, M. N. Mahyuddin, S. G. Khan, and C. Melhuish, "Robotic hand posture and compliant grasping control using operational space and integral sliding mode control," *Robotica*, vol. 34, no. 10, pp. 2163-2185, 2016, doi: 10.1017/S0263574714002811.

[10] O. Jedda, J. Ghabi, and A. Douik, "Sliding mode control of an inverted pendulum," *Applications of Sliding Mode Control*, pp. 105-118, 2017.

[11] D. Fulwani and B. Bandyopadhyay, "Design of sliding mode controller with actuator saturation," in *Advances in Sliding Mode Control: Concept, Theory and Implementation*, pp. 207-219, 2013.

[12] H. Obeid, L. M. Fridman, S. Laghrouche, and M. Harmouche, "Barrier function-based adaptive sliding mode control," *Automatica*, vol. 93, pp. 540-544, 2018, doi: 10.1016/j.automatica.2018.03.078.

[13] A. Samanfar, M. R. Shakarami, J. Soltani Zamani, and E. Rokrok, "Adaptive sliding mode control for multi-machine power systems under normal and faulted conditions," *Scientia Iranica*, vol. 29, no. 5, pp. 2526-2536, 2022, doi: 10.24200/sci.2020.55717.4371.

[14] M. Labbadi and M. Cherkaoui, "Robust adaptive backstepping fast terminal sliding mode controller for uncertain quadrotor UAV," *Aerospace Science and Technology*, vol. 93, p. 105306, 2019.

[15] F. Mohd Zaihidee, S. Mekhilef, and M. Mubin, "Robust speed control of PMSM using sliding mode control (SMC)—A review," *Energies*, vol. 12, no. 9, p. 1669, 2019, doi:10.3390/en12091669

[16] S. Jung, "Improvement of tracking control of a sliding mode controller for robot manipulators by a neural network," *International Journal of Control, Automation and Systems*, vol. 16, no. 2, pp. 937-943, 2018.

[17] S. Fan, H. Gu, Y. Zhang, M. Jin, and H. Liu, "Research on adaptive grasping with object pose uncertainty by multi-fingered robot hand," *International Journal of Advanced Robotic Systems*, vol. 15, no. 2, 2018.

[18] X. Li, Z. Chen, and C. Ma, "Optimal grasp force for robotic grasping and in-hand manipulation with impedance control," *Assembly Automation*, vol. 41, no. 2, pp. 208-220, 2021.

[19] E. Shahriari, S. A. B. Birjandi, and S. Haddadin, "Passivity-based adaptive force-impedance control for modular multi-manual object manipulation," *IEEE Robotics and Automation Letters*, vol. 7, no. 2, pp. 2194-2201, 2022.

[20] T. Zhang, L. Jiang, S. Fan, X. Wu, and W. Feng, "Development and experimental evaluation of multi-fingered robot hand with adaptive impedance control for unknown environment grasping," *Robotica*, vol. 34, no. 5, pp. 1168-1185, 2016.

[21] S. M. Mahdi, N. Q. Yousif, A. A. Oglah, M. E. Sadiq, A. J. Humaidi, and A. T. Azar, "Adaptive synergetic motion control for wearable knee-assistive system: a rehabilitation of disabled patients," in *Actuators*, vol. 11, no. 7, p. 176, 2022, doi: 10.3390/act11070176.

[22] Shadow Robot Company, "Shadow dexterous hand technical specification, *Shadow Robot Company*, 2022.

[23] S. A. Ajwad, R. U. Islam, M. R. Azam, M. I. Ullah, and J. Iqbal, "Sliding mode control of rigid-link anthropomorphic robotic arm," in *2016 2nd International Conference on Robotics and Artificial Intelligence (ICRAI)*, pp. 75-80, 2016.

[24] S. S. Ali, S. M. Raafat, and A. Al-Khazraji, "Improving the performance of medical robotic system using H∞ loop shaping robust controller," *International Journal of Modelling, Identification and Control*, vol. 34, no. 1, pp. 3-12, 2020.

[25] A. S. Ahmed and S. K. Kadhim, "Non-Leaner Control on the Pneumatic Artificial Muscles: A Comparative Study Between Adaptive Backstepping and Conventional Backstepping Algorithms," *Mathematical Modelling of Engineering Problems*, vol. 10, no. 2, 2023, doi: 10.18280/mmep.100236.

[26] S. A. Emam, "Generalized Lagrange's equations for systems with general constraints and distributed parameters," *Multibody System Dynamics*, vol. 49, pp. 95-117, 2020.

[27] R. Dhaouadi and A. A. Hatab, "Dynamic modelling of differential-drive mobile robots using lagrange and newton-euler methodologies: A unified framework," *Advances in robotics & automation*, vol. 2, no. 2, pp. 1-7, 2013, doi: 10.4172/2168-9695.1000107.

[28] C. Armenta-Déu and H. Cortés, "Analysis of kinetic energy recovery systems in electric vehicles," *Vehicles*, vol. 5, no. 2, pp. 387-403, 2023, doi: 10.3390/vehicles5020022.

[29] H. El-Hussieny, S. G. Jeong, and J. H. Ryu, "Dynamic modeling of a class of soft growing robots using euler-lagrange formalism," *Society of Instrument and Control Engineers*, 2019.

[30] M. W. Spong, S. Hutchinson, and M. Vidyasagar. *Robot modeling and control*. John Wiley & Sons, 2020.

[31] A. S. Ahmed and S. K. Kadhim, "A comparative study between convolution and optimal backstepping controller for single arm pneumatic artificial muscles," *Journal of Robotics and Control (JRC)*, vol. 3, no. 6, pp. 769-778, 2022, doi: 10.18196/jrc.v3i6.16064.

[32] N. B. Almutairi and M. Zribi, "Sliding mode control of a three-dimensional overhead crane," *Journal of Vibration and Control Overhead Crane*, vol. 15, no. 11, pp. 1679–1730, 2009.

[33] D. H. Tu'ma and A. K. Hamoudi, "Performance of 2-link robot by utilizing adaptive sliding mode controller," *Journal of Engineering*, vol. 26, no. 12, pp. 44-65, 2020.

[34] D. S. Shanan and S. K. Kadhim, "Comparative Analysis of Airflow Regulation in Ventilator Systems Using Various Control Strategies," *Journal Européen des Systèmes Automatisés*, vol. 56, no. 5, 2023, doi: 10.18280/jesa.560512.

[35] D. Sheltag and S. K. Kadhim, "Enhancing Artificial Ventilator Systems: A Comparative Analysis of Traditional and Nonlinear PID Controllers," *Mathematical Modelling of Engineering Problems*, vol. 11, no. 3, 2024, doi: 10.18280/mmep.110303.

[36] H. Benbouhenni, "Synergetic control theory scheme for asynchronous generator based dual-rotor wind power," *Journal of Electrical Engineering, Electronics, Control and Computer Science*, vol. 7, no. 3, pp. 19-28, 2021.

[37] Q. Junjie, L. Kaiting, W. Huaren, Y. Jianfei, and L. Xiaohui, "Syner getic control of grid-connected photovoltaic systems," *Int J Pho toenergy*, vol. 2017, p. 5051489, 2017, doi: 10.1155/2017/50514_89.

[38] E. Santi, A. Monti, D. Li, K. Proddutur, and R. A. Dougal, "Synergetic control for power electronics applications: A comparison with the sliding mode approach," *Journal of Circuits, Systems, and Computers*, vol. 13, no. 4, pp. 737-760, 2004.

[39] M. Harmas, A. Hamzaoui, K. Harmas, and Z. Bouchama, "Adaptive fuzzy synergetic converter control," in *1st Taibah University international conference on computing and information tech nology ICCIT 2012*, pp 734–738, 2012.

[40] Q. Wang, J. Feng, and T. Li, "Analysis of the Synergetic Control Based on Variable Structure and Application of Power Electronics," *Proc. - 2009 Int. Conf. Inf. Eng. Comput. Sci. ICIECS 2009*, no. 5, pp. 3–6, 2009, doi: 10.1109/ICIECS.2009.5367012.

[41] I. Kondratiev, E. Santi, R. Dougal, and R. Veselov, "Synergetic con trol for m-parallel connected dc–dc buck converters," in *PESC, 30th annual IEEE*, vol. 1, pp. 182–188, 2004.

[42] E. Santi, A. Monti, D. Li, K. Proddutur, and R. A. Dougal, "Synergetic control for DC-DC boost converter: implementation options," *IEEE Transactions on industry applications*, vol. 39, no. 6, pp. 1803-1813, 2003.

[43] X. Ju, P. Zhao, H. Sun, W. Yao, and J. Wen, "Nonlinear synergetic governor controllers for steam turbine generators to enhance power system stability," *Energies*, vol. 10, no. 8, p. 1092, 2017, doi: 10.3390/en1008102.

[44] A. J. Humaidi, I. K. Ibraheem, A. T. Azar, and M. E. Sadiq, "A new adaptive synergetic control design for single link robot arm actuated by pneumatic muscles," *Entropy*, vol. 22, no. 7, p. 723, 2020.

[45] A. F. Mutlak and A. J. Humaidi, "A Comparative Study of Synergetic and Sliding Mode Controllers for Pendulum Systems," *Journal Européen des Systèmes Automatisés*, vol. 56, no. 5, 2023, doi: 10.18280/jesa.560518.

[46] A. Q. Al-Dujaili, A. J. Humaidi, Z. T. Allawi, and M. E. Sadiq, "Earthquake hazard mitigation for uncertain building systems based on adaptive synergetic control," *Applied system innovation*, vol. 6, no. 2, p. 34, 2023, doi: 10.3390/asi6020034.

[47] A. Rebai, K. Guesmi, and B. Hemici, "Adaptive fuzzy synergetic control for nonlinear hysteretic systems," *Nonlinear Dynamics*, vol. 86, pp. 1445-1454, 2016.

[48] A. J. Humaidi and A. H. Hameed, "Design and comparative study of advanced adaptive control schemes for position control of electronic throttle valve," *Information*, vol. 10, no. 2, p. 65, 2019, doi: 10.3390/info10020065.

[49] A. Kanchanaharuthai and E. Mujjalinvimut, "Application of adaptive synergetic control to power systems with superconducting magnetic energy storage system," *International Journal of Innovative Computing, Information and Control*, vol. 13, no. 6, pp. 1873-1885, 2017.

[50] Q. Xu, "Precision motion control of piezoelectric nanopositioning stage with chattering-free adaptive sliding mode control," *IEEE Transactions on Automation Science and Engineering*, vol. 14, no. 1, pp. 238-248, 2016.

[51] A. Kanchanaharuthai and E. Mujjalinvimut, "Adaptive finite-time synergetic control design for power systems with static var compensator," *Int. J. innovative Comput., Inf. Control: IJICIC*, vol. 16, pp. 1007-1020, 2020.

[52] H. S. Majeed, S. K. Kadhim, and A. A. Jaber, "Design of a sliding mode controller for a prosthetic human hand's finger," *Engineering and Technology Journal*, vol. 40, no. 1, pp. 257-266, 2022, doi: 10.30684/etj.v40i1.1943.

[53] A. M. Hameed and A. K. Hamoudi, "A 2-Link Robot with Adaptive Sliding Mode Controlled by Barrier Function," *Journal Européen des Systèmes Automatisés*, vol. 56, no. 6, 2023, doi: 10.18280/jesa.560620.

[54] H. Zhou and J. Zhai, "Adaptive Sliding Mode Control with Disturbance Observer for Trajectory Tracking of Robotic Milling," in *Chinese Intelligent Systems Conference* (pp. 643-652, 2023, doi: 10.1007/978-981-99-6886-2_55.

[55] S. Yi and J. Zhai, "Adaptive second-order fast nonsingular terminal sliding mode control for robotic manipulators," *ISA transactions*, vol. 90, pp. 41-51, 2019, doi: 10.1016/j.isatra.2018.12.046.

[56] Z. Li, J. Zhai, and H. R. Karimi, "Adaptive finite-time super-twisting sliding mode control for robotic manipulators with control backlash," *International Journal of Robust and Nonlinear Control*, vol. 31, no. 17, pp. 8537-8550, 2021, doi: 10.1002/rnc.5744.

[57] S. Abulanwar, A. Ghanem, M. E. Rizk, and W. Hu, "Adaptive synergistic control strategy for a hybrid AC/DC microgrid during normal operation and contingencies," *Applied Energy*, 304, p. 117756, 2021, doi: 10.1016/j.apenergy.2021.117756.

[58] D. Al-hadithy and A. Hammoudi, "Two-link robot through strong and stable adaptive sliding mode controller," in *2020 13th International Conference on Developments in eSystems Engineering (DeSE)*, pp. 121-127, 2020, doi: 10.1109/DeSE51703.2020.9450762.

[59] M. A. Salman and S. K. Kadhim, "Optimal backstepping controller design for prosthetic knee joint," *Journal Européen des Systèmes Automatisés*, vol. 55, no. 1, pp. 49-59, 2022, doi: 10.18280/jesa.550105.

[60] R. C. D. Hora, S. D. S. Lima, and S. H. D. C. Santos, "Moving mass/load speed influence on the structural dynamic response of a bridge," *Revista IBRACON de Estruturas e Materiais*, vol. 16, p. e16601, 2023, doi: 10.1590/S1983-41952023000600001.